NRL Report 8370

Fractographic and Microstructural Analysis of SCC Specimens of HY-100, HY-130, and HY-180 Steel Weldments

FRANCES W. FRASER AND EDWARD A. METZBOWER

Advanced Materials Technology Branch
Material Science and Technology Division

January 10, 1980

NAVAL RESEARCH LABORATORY
Washington, D.C.

Approved for public release; distribution unlimited.

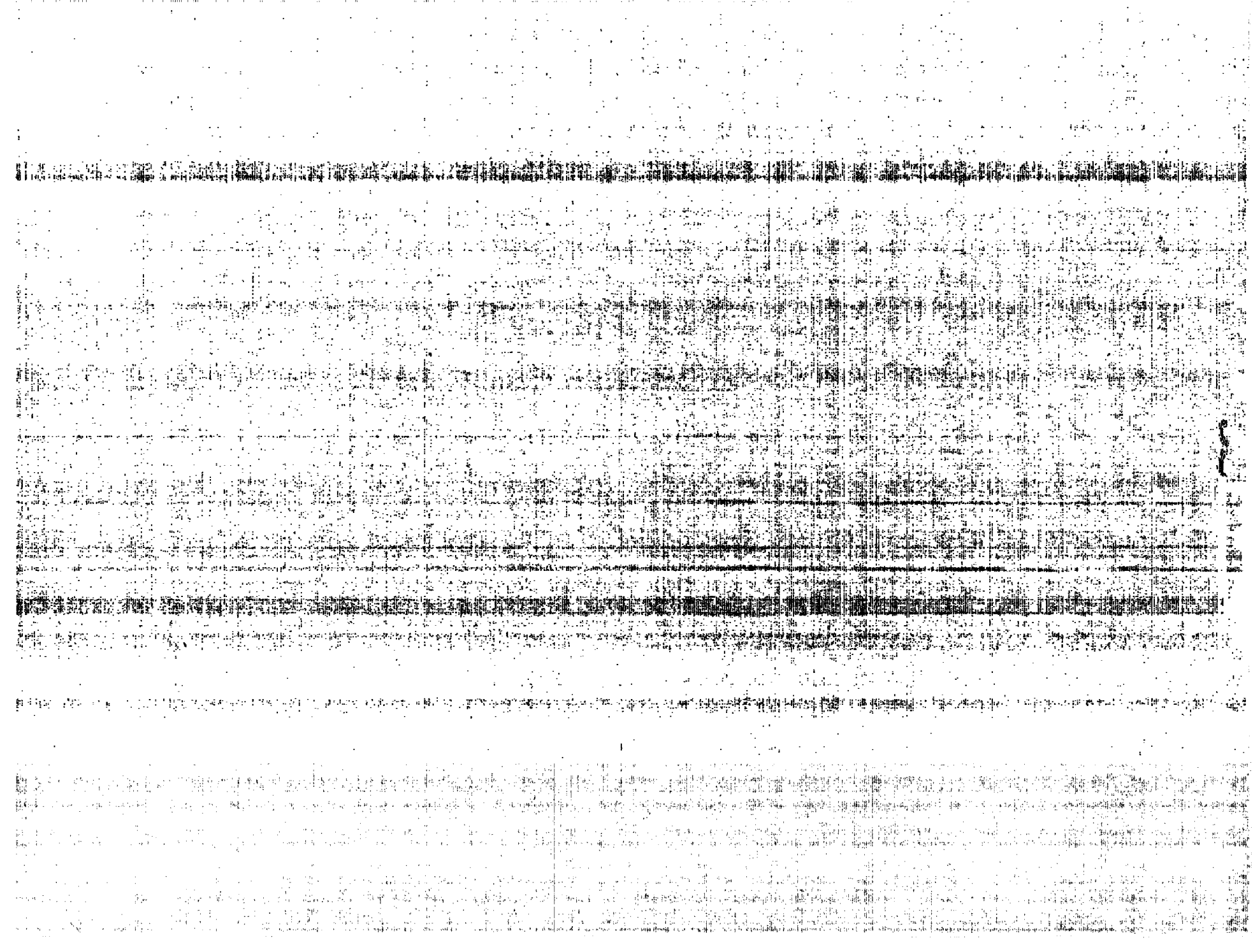

REPORT DOCUMENTATION PAGE

READ INSTRUCTIONS BEFORE COMPLETING FORM

1. REPORT NUMBER: NRL Report 8370
2. GOVT ACCESSION NO.:
3. RECIPIENT'S CATALOG NUMBER:

4. TITLE (and Subtitle): FRACTOGRAPHIC AND MICROSTRUCTURAL ANALYSIS OF SCC SPECIMENS OF HY-100, HY-130, AND HY-180 STEEL WELDMENTS

5. TYPE OF REPORT & PERIOD COVERED: Final report on one phase of a continuing NRL problem

6. PERFORMING ORG. REPORT NUMBER:

7. AUTHOR(s): Frances W. Fraser and Edward A. Metzbower

8. CONTRACT OR GRANT NUMBER(s):

9. PERFORMING ORGANIZATION NAME AND ADDRESS: Naval Research Laboratory, Washington, DC 20375

10. PROGRAM ELEMENT, PROJECT, TASK AREA & WORK UNIT NUMBERS: NRL Problem 1018-0, Project SF-54-591-500

11. CONTROLLING OFFICE NAME AND ADDRESS: Naval Ship Systems Command, Washington, DC 20362

12. REPORT DATE: January 10, 1980

13. NUMBER OF PAGES: 31

14. MONITORING AGENCY NAME & ADDRESS(if different from Controlling Office):

15. SECURITY CLASS. (of this report): UNCLASSIFIED

15a. DECLASSIFICATION/DOWNGRADING SCHEDULE:

16. DISTRIBUTION STATEMENT (of this Report): Approved for public release; distribution unlimited

17. DISTRIBUTION STATEMENT (of the abstract entered in Block 20, if different from Report):

18. SUPPLEMENTARY NOTES:

19. KEY WORDS (Continue on reverse side if necessary and identify by block number):

Fractography
Microstructure
Stress-corrosion cracking
Weld metal
HY-100 steel
HY-130 steel
HY-180 steel

20. ABSTRACT (Continue on reverse side if necessary and identify by block number):

This report summarizes an investigation of the microstructures and fracture morphologies of selected double-V weldments of HY-100, HY-130, and HY-180 steels fractured under stress in an aqueous environment. The specimens, which were prepared using substantially different welding practices and filler materials, displayed similar K_{Iscc} values. Optical examination of the microstructures showed that repeated thermal cycling, which occurs during fabrication of GTA (gas-tungsten-arc) fine-bead as-welded specimens, resulted in a uniform, fine-grained, tempered microstructure that

(Continues)

20. Abstract (Continued)

offered the greatest resistance to stress-corrosion cracking (SCC). Microvoid coalescence (MVC) was the dominant fracture mode.

Coarse-bead, as-welded, GMA (gas-metal-arc) specimens contained substantial amounts of high-temperature-transformation products which fractured by cleavage. Heat treating these specimens, to a lower yield strength, refined the microstructure and improved the SCC resistance. The dominant fracture mode of the heat-treated specimens was MVC. Microbranching of the advancing crack front occurred in the coarse-bead, as-welded specimens and may be responsible for the relatively high K_{Iscc} values reported.

CONTENTS

FRACTOGRAPHIC AND MICROSTRUCTURAL ANALYSIS OF SCC SPECIMENS OF HY-100, HY-130, and HY-180 STEEL WELDMENTS

INTRODUCTION

The critical-stress-intensity factor for crack initiation, K_{Iscc}, is used to evaluate the resistance of welded steels to subcritical crack growth. Stress-corrosion-cracking (SCC) behavior depends ultimately on the susceptibility of the microstructure and fracture paths. Variables such as chemical composition, thermal treatment, and welding processes and parameters alter the microstructures of materials and hence can be expected to affect the materials' resistances to SCC. This report summarizes an investigation of the fracture morphologies and the microstructures of selected double-V weldments of HY-100, HY-130, and HY-180 steels. Although prepared using substantially different welding practices and filler materials, the specimens analyzed displayed similar K_{Iscc} values in short-time (100-hour step load) screening tests. SCC testing was carried out with each specimen coupled to a sacrifical anode and fractured under stress in an aqueous environment.

MATERIALS AND PROCEDURE

Table 1 lists the identifying symbols, welding processes, heat treatments, welding electrodes, heat inputs, yield strengths, and K_{Iscc} values for weldments of each of the three steels investigated.

All of the analyzed specimens were single-edge notched and fatigue precracked. They were tested for stress-corrosion cracking in nonflowing 3.5% NaCl solution while galvanically coupled to Zn [1,2]. Testing was at room temperature.

One fracture surface of each specimen was stripped with replicating tape and then cleaned ultrasonically. If heavy rust deposits were encountered, the surface was cleaned with an acid containing an organic inhibitor, followed by thorough rinsing and ultrasonical cleaning.

After preliminary macroscopic examination, fractographic analyses were carried out in a scanning electron microscope (SEM). Subsequently each specimen was sectioned both longitudinally through the smooth or thermally cycled SCC area and transversely. The transverse section encompassed the coarse root pass area, where little or no thermal cycling had occurred, the smooth, thermally cycled area, and the final passes at the surface of the weldment.

The sections were mounted in Bakelite, polished, and etched. The Hy-100 and Hy-130 specimens were etched with 1% Nital, and the HY-180 specimens were etched with Kalling's reagent. Metallographic analyses were carried out on the polished and etched sections. In

Manuscript submitted October 4, 1979.

Table 1 — Treatments and Properties of the Specimens

Symbol‡	Welding Process*	Heat Treatment	Elec-trode	Heat Input (kJ/in.)	Yield Strength (MPa)	(ksi)	K_{Iscc} - 100 h† (MPa √m)	(ksi √in.)
HY-100 Steel								
Z	GTA	As welded	120S	39	931	135	110	100
A	GMA	As welded	120S	45	820	119	122	111
HY-130 Steel								
F	GTA	As welded	140S	29	1011	151	99	90
T	GTA	As welded	BMC	31	1018	152	126	115
G	GMA	As welded	BMC	45	938	136	101	92
K	GMA	At 816°C (1500°F) 1h, water quench (WQ); at 593°C (1100°F) 1 h, WQ	BMC	45	903	131	123	112
L	GMA	Stress relief embrittled at 552°C (1025°F) 98 h, furnace cooled	140S	45	1000	145	42	38
R	GMA	As welded	AX110	35	1034	150	109	99
E	SMA	As welded	14018	10	993	144	110	100
HY-180 Steel (10Ni)								
I	GTA	As welded (coarse bead)	BMC	86	1138	165	88	80
J	GTA	As welded (fine bead)	BMC	30	1296	188	89	81
Q	GTA	At 538°C (1000°F) 1h, WQ (fine bead)	BMC	30	1331	193	101	95
H	GTA	At 621°C (1150°F) 1h, WQ (fine bead)	BMC	30	862	125	130	118

*GTA = gas tungsten arc, GMA = gas metal arc, and SMA = shielded metal arc.
†Hold time between load increments.
‡Base-metal chemistry.

some instances the specimens were repolished and etched with 10% ammonium persulfate solution to reveal solidification substructure. Microstructures were identified by optical microscopy.

Hardnesses were measured with a Vicker's microhardness tester under a 300-g load. All measurements were converted to the Rockwell C scale (R_c).

RESULTS

HY-100 Weldments (Specimens Z and A)

Macroscopic examination of the HY-100 specimens showed pronounced plasticity in specimen Z. The SCC zone in specimen Z, except for the root pass area, was relatively smooth, whereas the SCC zone in specimen A contained brittle columnar areas in addition to smooth fracture regions (Figs. 1 and 2). Columnar grain areas were not distinguishable macroscopically on the fracture surface of specimen Z, and the overall appearance was more uniform and finer textured than that of specimen A. Both fracture surfaces showed voids or pores containing particulate matter. Short secondary cracks were found in the smooth areas on the surface of specimen A, whereas secondary cracking was not discernible macroscopically on the fracture surface of specimen Z.

On a microscopic scale specimen A fractured almost exclusively by cleavage (Fig. 3a). Some areas were found to resemble stretched microvoids at the fatigue/SCC interface, and, although no extensive secondary cracking occurred, short microcracks and scattered pores were found at or near the fatigue/SCC interface (Fig. 3b). A minor amount of grain-boundary separation occurred in the columnar grain areas of the SCC zone.

Fig. 1 — Fracture surface of specimen Z, the HY-100 GTA weldment

Fig. 2 — Fracture surface of specimen A, the HY-100 GMA weldment

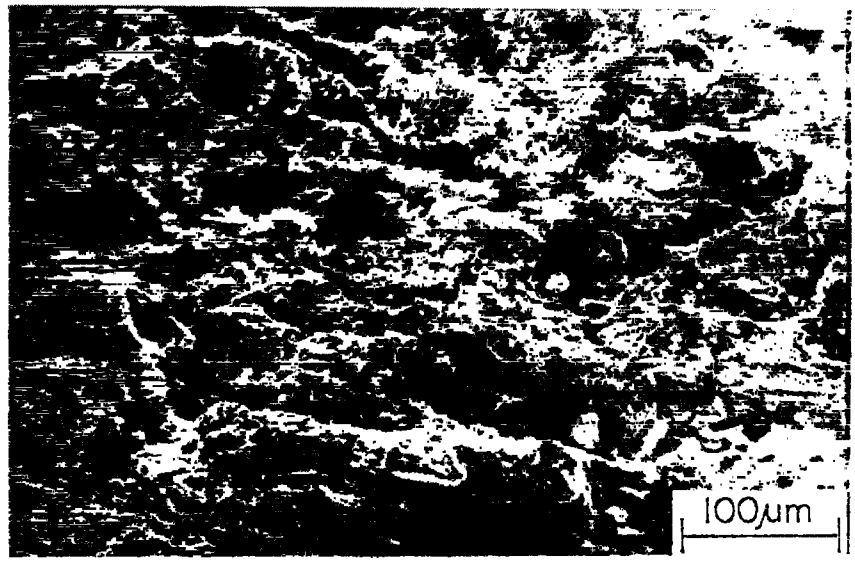

Fig. 3a — Fracture by cleavage in specimen A

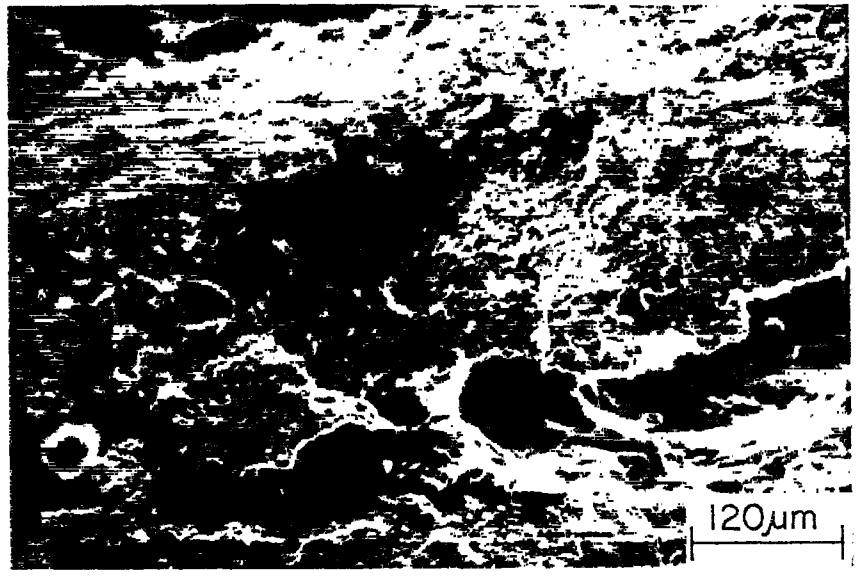

Fig. 3b — Fatigue/SCC interface showing microcracks and pores in specimen A

Specimen Z fractured by cleavage and microvoid coalescence (MVC). No secondary cracking was found at the fatigue/SCC interface, and no microcracks were seen in the SCC zone in general. Fast fracture in both specimens occurred by MVC.

The microstructure of each specimen was predominantly a mixture of ferrite and either bainite or baintic ferrite and carbides. The ferrite morphology in specimen A was largely acicular, and a network, or vein, of ferrite was found along some grain boundaries (Fig. 4a). Also, the ferrite morphology in some areas resembled a Widmanstätten structure, and strings of enlarged, spheroidal particles were found along prior austenite grain boundaries (Fig. 4b). In specimen Z the microstructure was relatively fine and uniform (Fig. 5) with no evidence of a ferritic network at the grain boundaries. Secondary cracks, extending from the fracture edge into the microstructure, were prominent in specimen A but not in specimen Z. Grain-boundary separation, and the generally coarse texture of the columnar grain areas on the fracture surface of specimen A, probably resulted from cleavage of the ferritic networks.

The hardness of specimen Z, along the fracture edge, ranged from 24.7 R_c to 32.1 R_c, whereas the hardness of specimen A ranged from 28.4 R_c to 35.0 R_c. In specimen A the hardest areas were found within the coarse columnar grains.

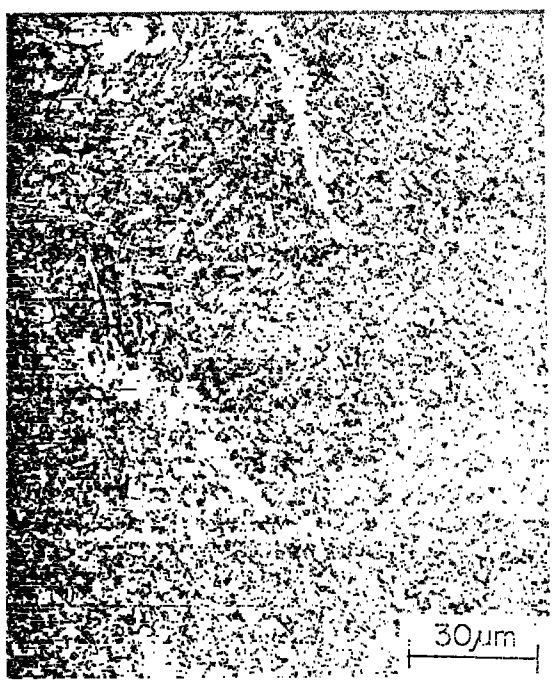

Fig. 4a — Ferrite veins at grain boundaries in specimen A

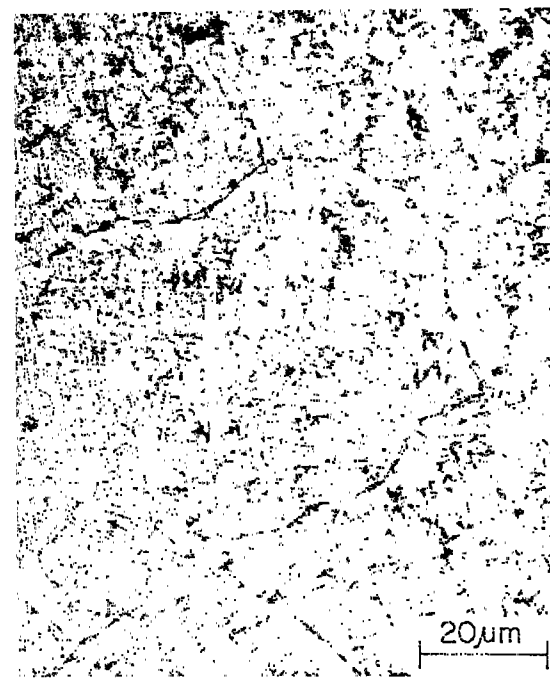

Fig. 4b — Widmanstätten structure and spheroidal grain-boundary particles in specimen A

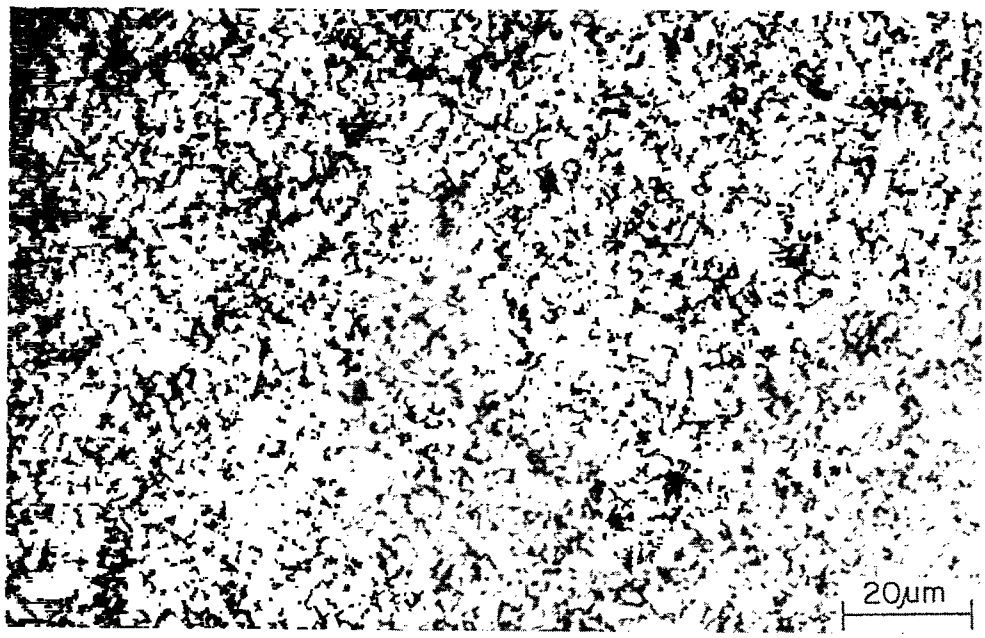

Fig. 5 — Uniform, fine-grained microstructure in specimen Z

HY-130 GTA Weldments (Specimens F and T)

The overall macroscopic appearance of the fracture surface of specimen F was smooth. The SCC area showed smooth, flat fracture except for the root pass area and embrittled areas at the specimen sides. The stress-corrosion crack appeared to have propagated inward from the sides of the specimen as well as from the fatigue crack. This accounts for the exaggerated, concave shape of the SCC zone (Fig. 6).

In general, the appearance of the fracture surface of specimen T (base-metal chemistry) was similar to that of specimen F except for extensive secondary cracks running horizontally through the SCC zone and for the less pronounced, concave shape of the zone (Fig. 7).

In specimen F, fracture in the smooth portions of the SCC zone occurred exclusively by MVC. The coarser root pass area fractured predominantly by cleavage, except in scattered areas where fracture occurred by MVC. The embrittled sides also fractured by cleavage. However, the microcracks in these areas were probably evidence of some columnar grain-boundary separation. Fast fracture occurred by MVC, with dimples ranging from fine to coarse. Secondary cracks were found in the smooth SCC area, the root pass area, and the fast-fracture area.

As in specimen F, fracture in specimen T occurred by MVC in the smooth SCC areas and by cleavage in both the root pass area and the embrittled areas at the sides of the specimen. Fast fracture occurred by MVC. The dimples on the fracture surface of specimen T were generally finer and more uniform than those on specimen F and may reflect the solidification substructure. Secondary cracking was considerably more extensive than in specimen

F. It occurred at the fatigue/SCC interface and, more prominently, at the SCC/fast-fracture interface. Secondary cracks were also found throughout the SCC and fast-fracture areas. Also, indications of grain-boundary separation were seen in the columnar grain zones of the SCC areas. Stretched zones had formed in conjunction with secondary cracks at the SCC/fast-fracture interface.

In both specimens the solidification structure was predominantly cellular; however, specimen F was considerably coarser than specimen T. Along the fracture edge of the longitudinal section, taken through the smooth SCC area of specimen T, the structure was very fine (Fig. 8) and in some areas was virtually unresolvable optically.

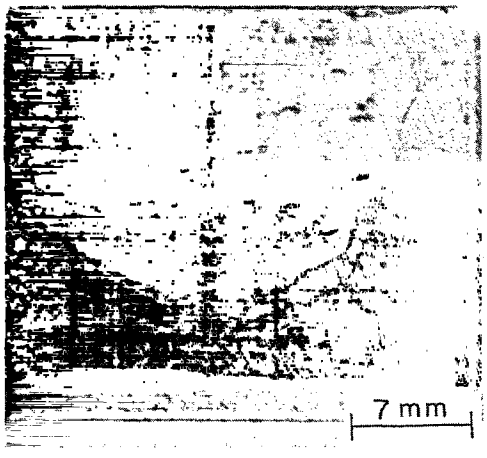

Fig. 6 — Fracture surface of specimen F, an HY-130 GTA weldment

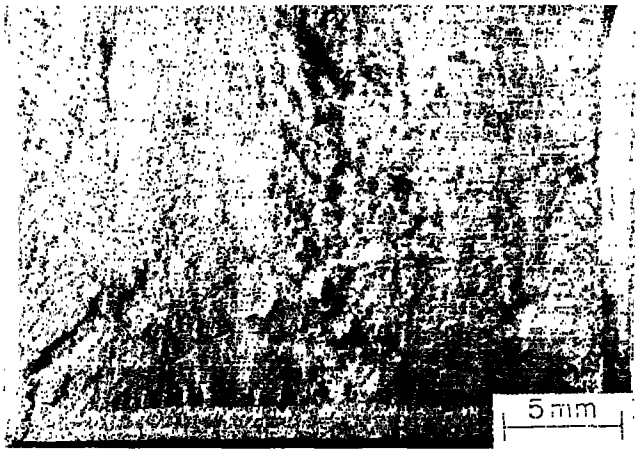

Fig. 7 — Fracture surface of specimen T, an HY-130 GTA weldment

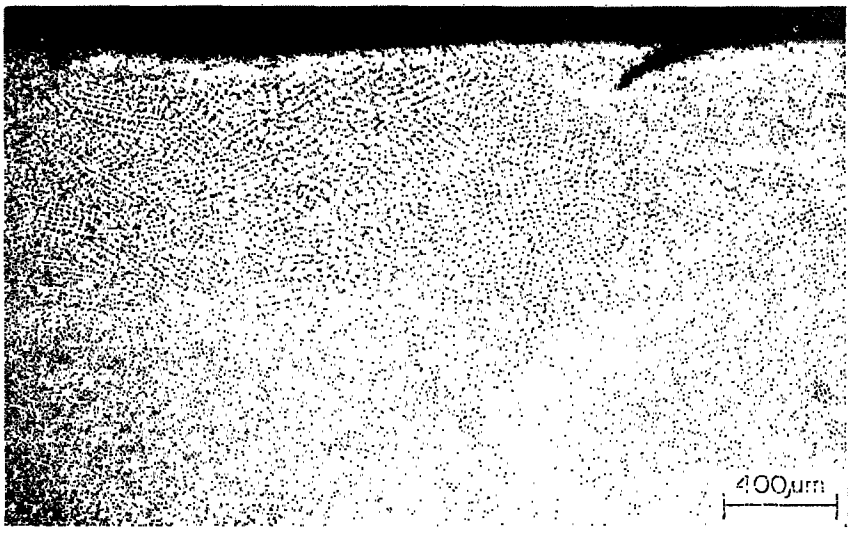

Fig. 8 — Solidification substructure along the fracture edge in the smooth SCC area in specimen T

The microstructure in specimen F was mixed. The smooth, thermally cycled areas were composed of fine-grained, tempered martensite, blocky ferrite, and some bainite (Fig. 9a), whereas the coarser grained areas, near the root pass, consisted of autotempered martensite, acicular ferrite, and bainite (Fig. 9b).

The microstructure in specimen T was similar to that in specimen F but with a finer, more uniform grain size in the smooth, thermally cycled areas (Fig. 10). As in specimen F, the microstructure in these areas was a mixture of tempered martensite, ferrite, and bainite. In the coarser, columnar grain areas the microstructure consisted of autotempered martensite and bainitic ferrite and carbides.

The polished and etched section of specimen T contained more microvoids than did the polished and etched section of specimen F, and some crack microbranching was noted in specimen T but not in specimen F.

The hardness of the weld metal along the fracture edge of specimen F ranged from 35.5 R_c to 37.9 R_c. The hardness range in specimen T was from 32.6 R_c to 37.2 R_c.

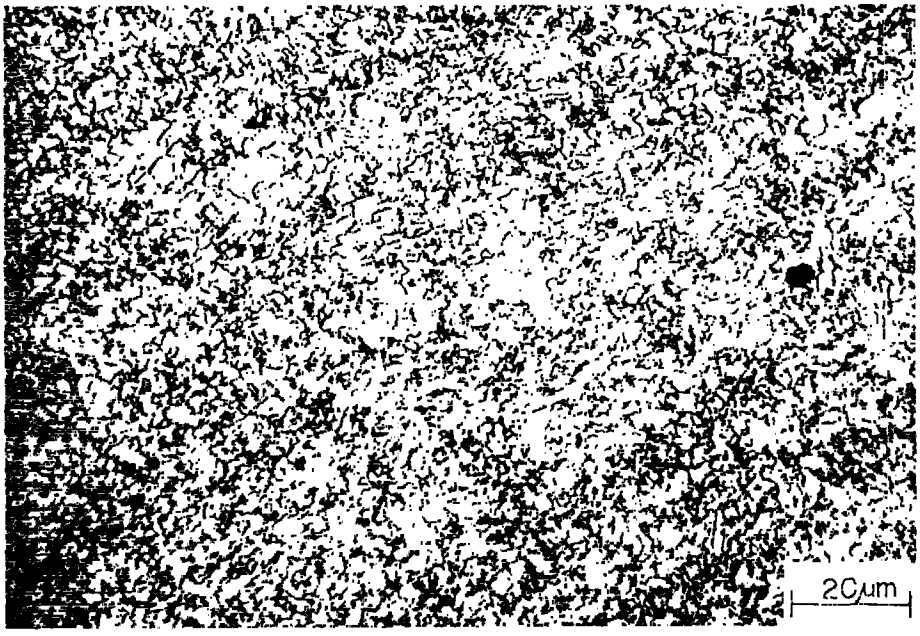

Fig. 9a — Fine-grained microstructure in the smooth SCC area in specimen F, consisting of tempered martensite, blocky ferrite, and bainite

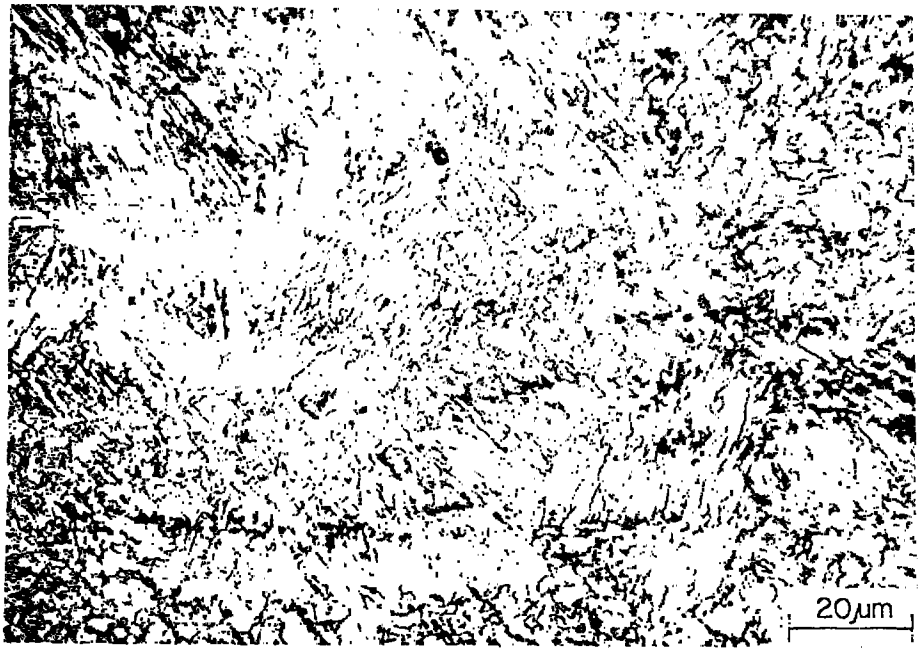

Fig. 9b — Coarse-grained microstructure near the root pass area in specimen F, consisting of autotempered martensite, acicular ferrite, and bainite

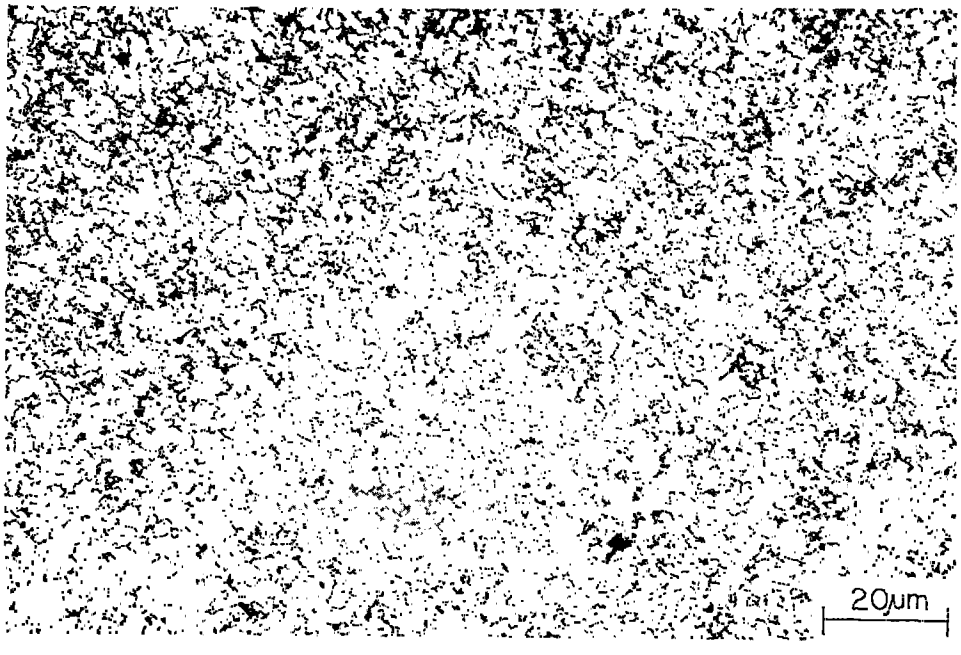

Fig. 10 — Fine grained microstructure in the smooth SCC area in specimen T, consisting of tempered martensite, ferrite, and bainite

HY-130 GMA Weldments (Specimens G, K, L, and R)

Macroscopic examination of specimen G showed smooth-textured, flat areas as well as rough, coarse-textured areas across the fracture surface in both the SCC and fast-fracture regions (Fig. 11). The SCC zone was of relatively uniform depth with no indication of extension along the weldment sides.

Specimen K, a heat-treated HY-130 specimen, exhibited a similar macrofracture appearance. Both coarse-textured and fine-textured areas were observed across the fracture surface; however, an SCC zone could not be detected macroscopically (Fig. 12).

Fracture in the SCC areas of specimen G, an as-welded HY-130 specimen, occurred by cleavage and MVC. Cleavage facets in the smooth SCC areas were relatively fine. In the rough-textured SCC regions—the columnar grain areas (Fig. 13) and the root pass area—the facets were coarse. Extensive secondary cracking was found in the root pass area, whereas short microcracks were found in the smooth SCC areas. There was no evidence of intergranular (IG) fracture. Stretch zones were found at both the fatigue/SCC interface and the SCC/fast-fracture interface. Microvoids containing inclusions were found in both the SCC and fast-fracture areas. Fast fracture occurred primarily by MVC with dimples that appeared relatively fine and uniform as compared to those seen in the SCC area. Cleavage and secondary cracks were found at scattered locations within the fast-fracture portion of the specimen.

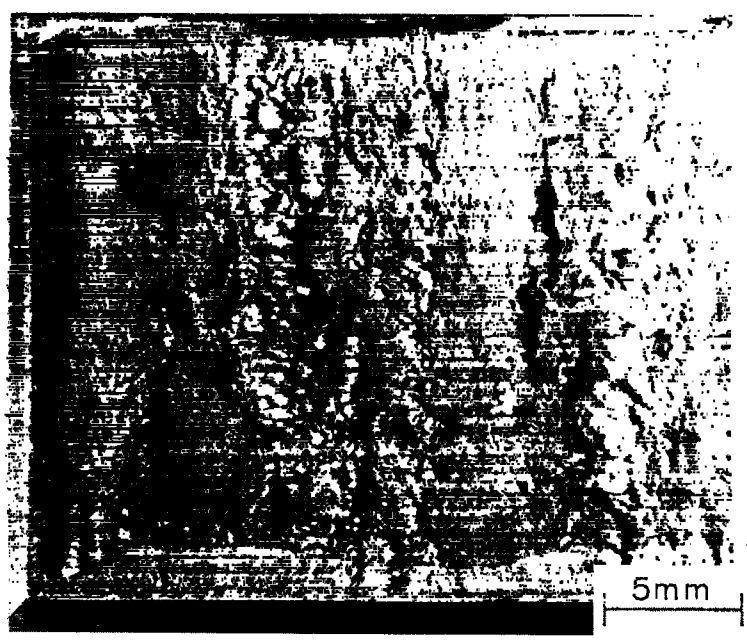

Fig. 11 — Fracture surface of specimen G, an HY-130 GMA weldment

In specimen K, a heat-treated HY-130 specimen, fracture modes at the fatigue interface included IG separation, cleavage, and MVC. Some IG fracture occurred in columnar grain and adjacent equiaxed grain areas (Figs. 14a and 14b). Smooth, flat areas fractured by MVC, which was accompanied in some instances by stretching, whereas the coarser areas fractured by MVC and cleavage. Microcracks, corrosion products, and pitting were also noted.

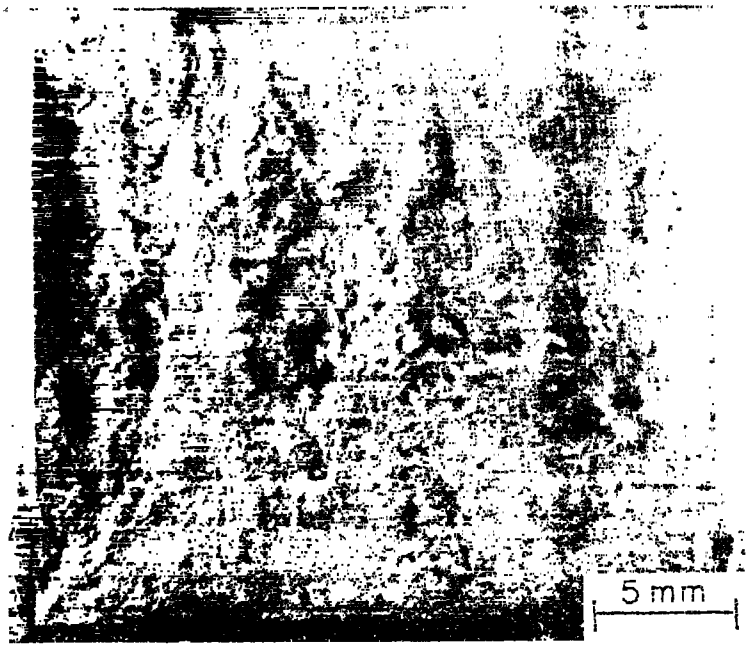

Fig. 12 — Fracture surface of specimen K, an HY-130 heat-treated weldment

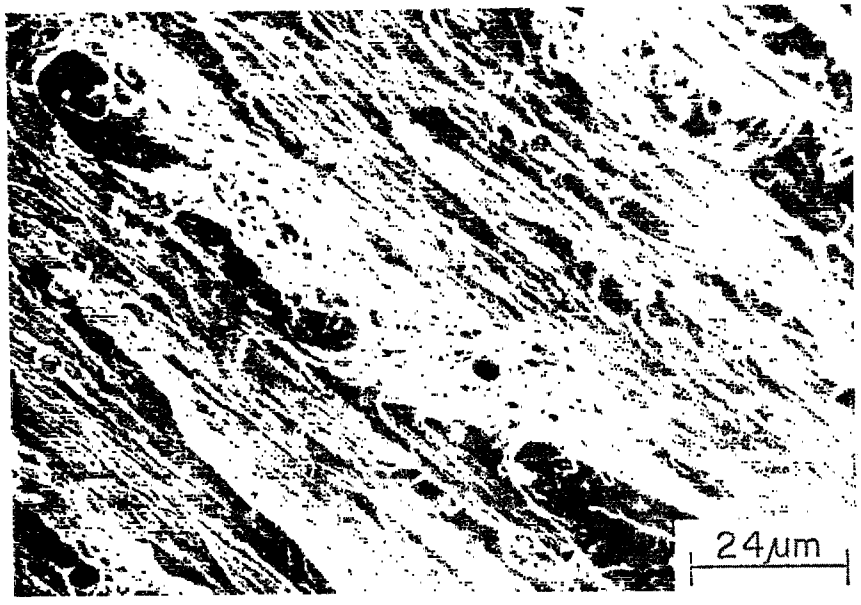

Fig. 13 — Cleavage and MVC in the coarse columnar-grain area within the SCC zone in specimen G

Fig. 14a — Intergranular separation in columnar grains in specimen K

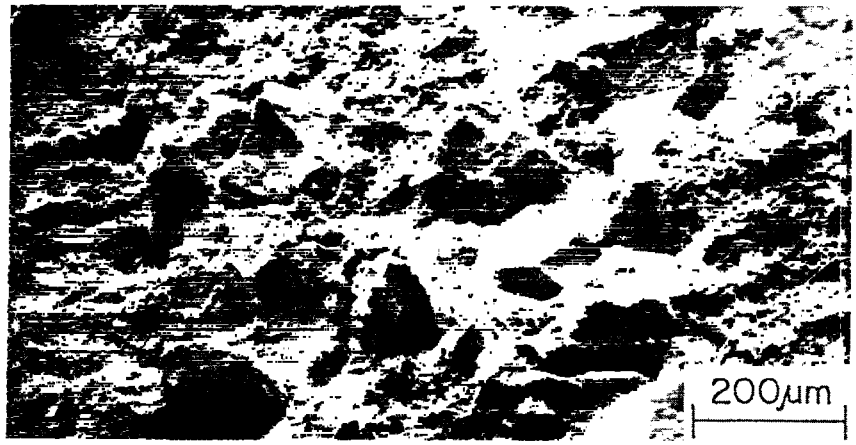

Fig. 14b — Intergranular separation in equiaxed grains in specimen K adjacent to the columnar grains in Fig. 14a

There was no clear demarcation between an SCC area and a fast-fracture area. A filmlike surface and fracture markings resembling a solidification pattern were found on the faces of some of the columnar grains (Fig. 15). In areas of MVC, the dimples ranged from fine to coarse, and many contained inclusions.

The microstructure of specimen G was generally coarse. It consisted of mixed acicular and blocky ferrite, martensite which had undergone varying degrees of tempering, and bainitic aggregates of ferrite and coarse carbides (Fig. 16). Microcracks were found within the microstructure along with voids of various sizes.

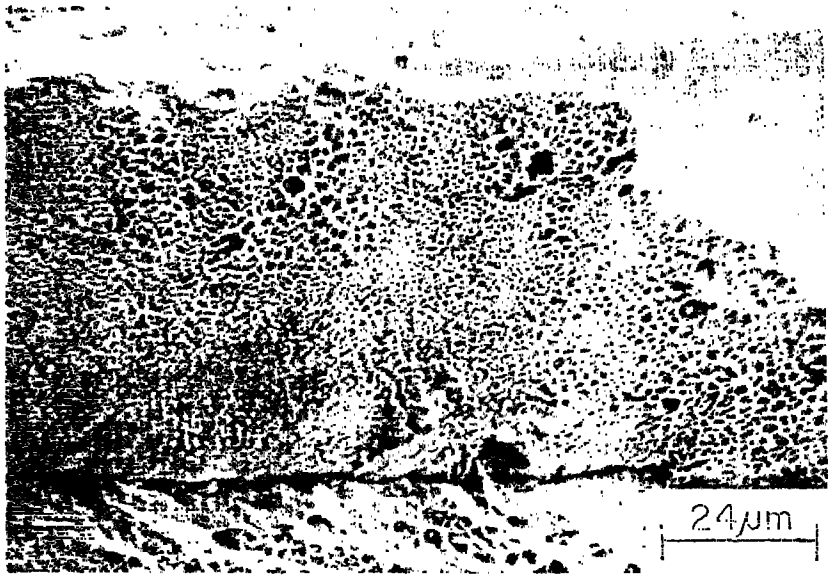

Fig. 15 — Filmlike surface on the face of the columnar grains in specimen K

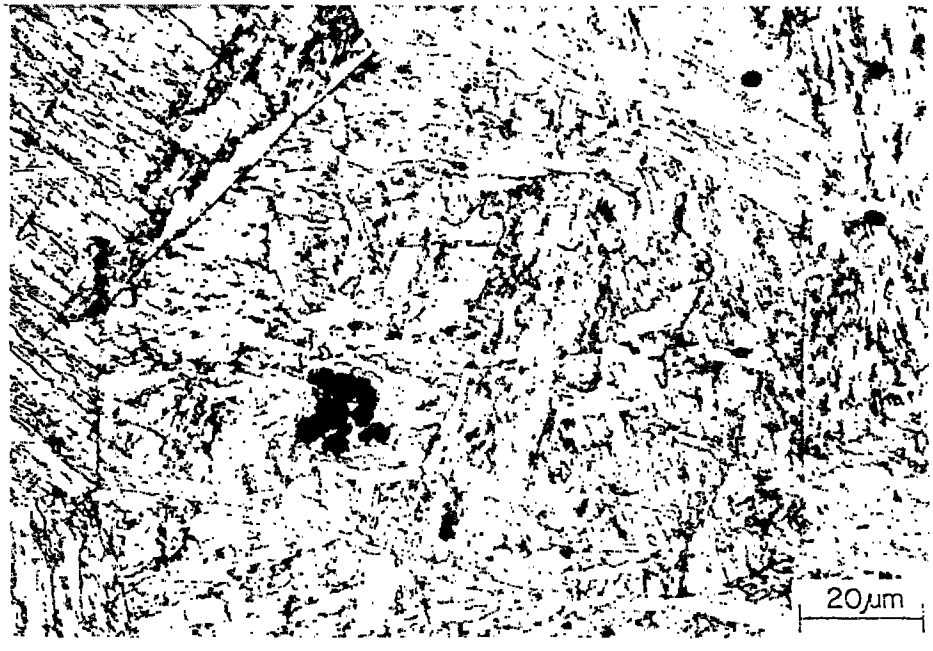

Fig. 16 — Microstructure composed of martensite, ferrite, and bainite in specimen G

The microstructure of specimen K was of a smaller grain size and generally finer than that of specimen G. It was composed of tempered martensite, acicular ferrite, and scattered areas of bainite and coalesced carbides (Fig. 17).

At the fracture edge, hardness measurements ranged from 31.1 R_c to 33.0 R_c in specimen G and from 30.0 R_c to 34.0 R_c in specimen K.

A macrograph of the fracture surface of temper-embrittled specimen L is shown in Fig. 18. Bands consisting of elongated columnar grains, areas of smooth, flat fracture, and faceted grains alternate across the fracture surface. Neither a fatigue zone nor an SCC zone could be discerned macroscopically. This specimen fractured predominantly by IG separation and cleavage, with some ductile tearing between brittle ridges.

The microstructure consisted of martensite, acicular ferrite, and bainite. Ferrite platelets, along with clusters of precipitates, formed at the boundaries of the more equiaxed grains (Fig. 19). Strings of precipitates and microcracks were found along columnar grain boundaries.

Hardness values along the fracture edge ranged from 32.1 R_c to 34.6 R_c.

The fracture surface of specimen R was generally rough and coarse textured (Fig. 20). It was characterized mainly by elongated columnar grains and coarse faceted areas but with some fine, smooth fibrous regions. Voids or gas pockets were prominent in the fast-fracture area. The SCC zone contained crevices and large pockets which were not confined to the

Fig. 17 — Microstructure composed of acicular ferrite, bainite, and coalesced carbides in specimen K

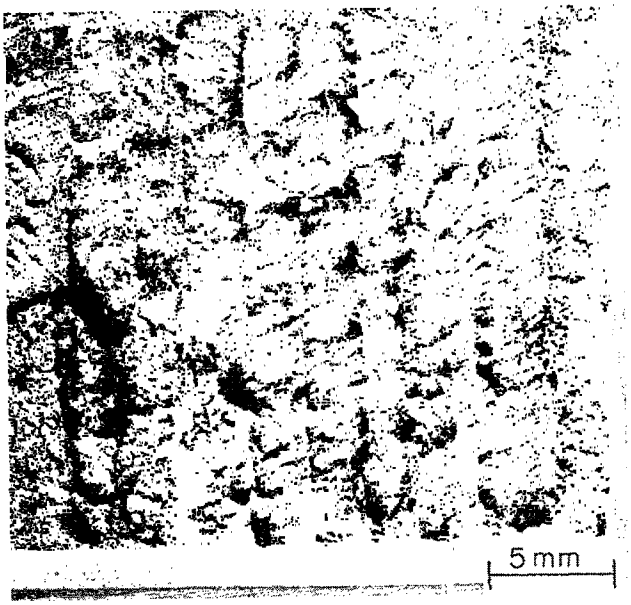

Fig. 18 — Fracture surface of specimen L, the HY-130 temper-embrittled, GMA weldment

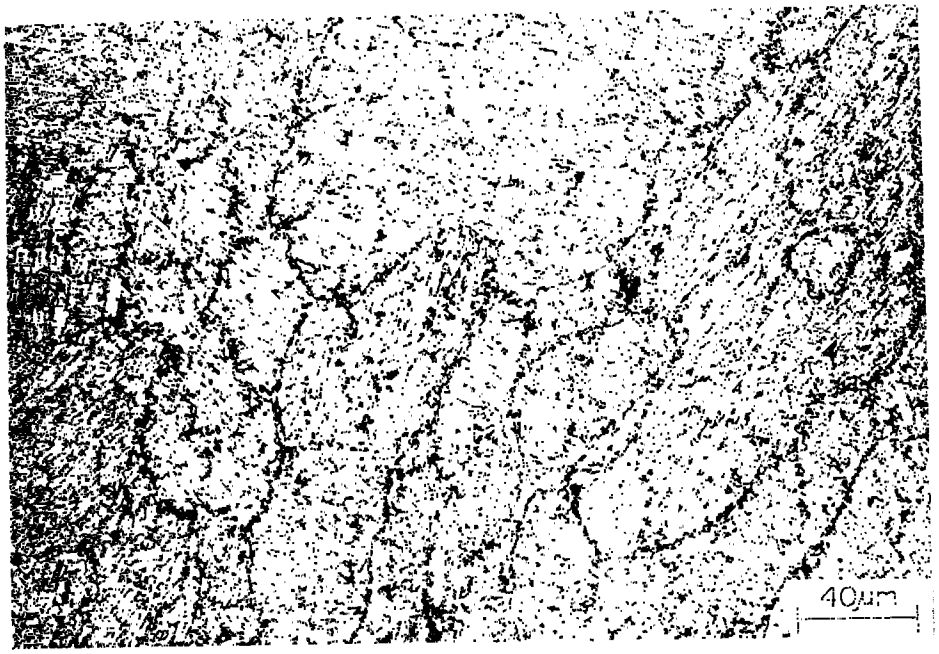

Fig. 19 — Microstructure showing ferrite platelets and precipitates along grain boundaries in specimen L

Fig. 20 — Fracture surface of specimen R, an HY-130 GMA weldment

root pass area. Embrittlement of the weld metal was seen along the sides of the specimen, along with corroded areas in both the SCC and fatigue zones.

In the SCC area, fracture occurred by IG separation, cleavage, and MVC. Microcracks were found along the fatigue/SCC interface. Fracture along this interface occurred by cleavage and MVC. IG separation was found in the root pass area and along the embrittled sides of the specimen. Stretched dimples were prominent along the SCC/fast-fracture interface. Fast fracture occurred predominantly by MVC, but some cleavage occurred in the coarse, columnar-grain areas. Precipitates were generally found within the microvoids. Solidification substructure could be identified within the voids found in the fast-fracture area. Some contained a single, relatively large inclusion (Fig. 21) which was determined by energy dispersive x-ray analysis to contain Mn, Ti, and Si.

The microstructure, which was similar to that of specimen G but finer, consisted of bainitic ferrite and carbides, martensite that had undergone varying degrees of tempering, and acicular ferrite (Fig. 22a). In addition to branched microcracks which extended from the fracture edge into the microstructure, isolated cracks and coalesced carbides were found throughout the microstructure.

In this specimen the solidification structure along the fracture edge was predominantly dendritic (Fig. 22b). It was relatively coarse and contained solute pools, which in a previous investigation were found to be evidence of microsegregation [3]. Hardness values ranged from 35.8 R_c to 40.2 R_c.

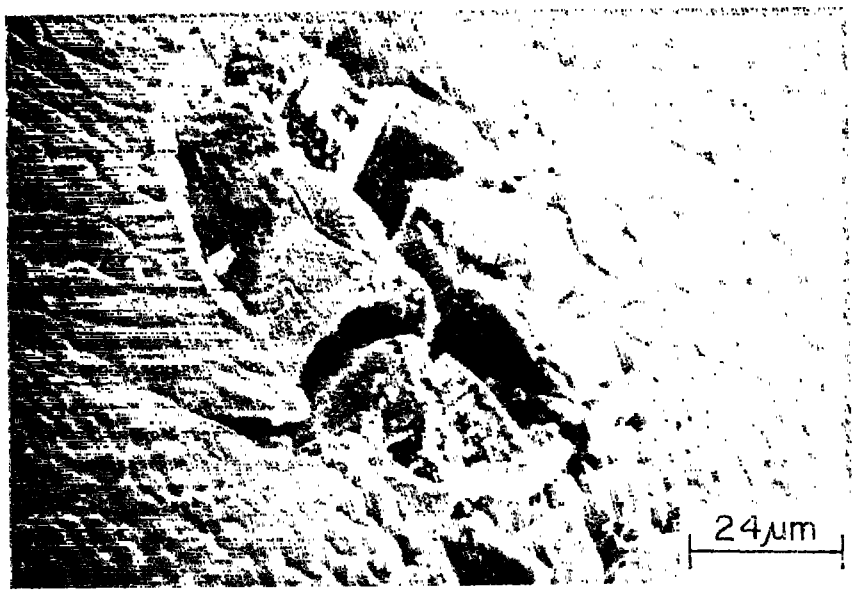

Fig. 21 — Inclusion within a void in the fast-fracture area in specimen R and solidification structure around the inclusion

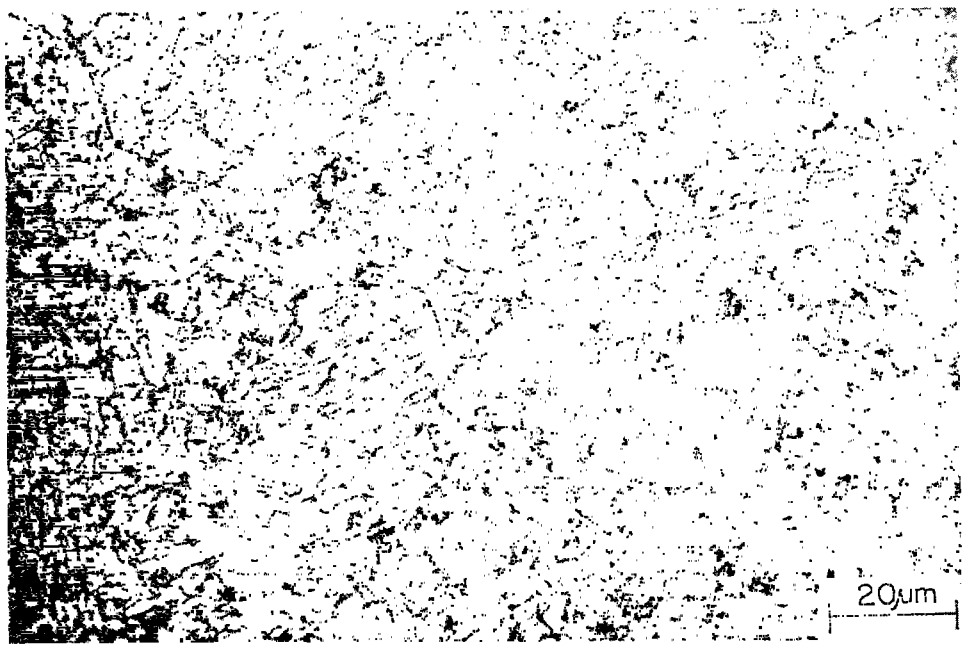

Fig. 22a — Acicular ferrite, bainite, and martensite in specimen R

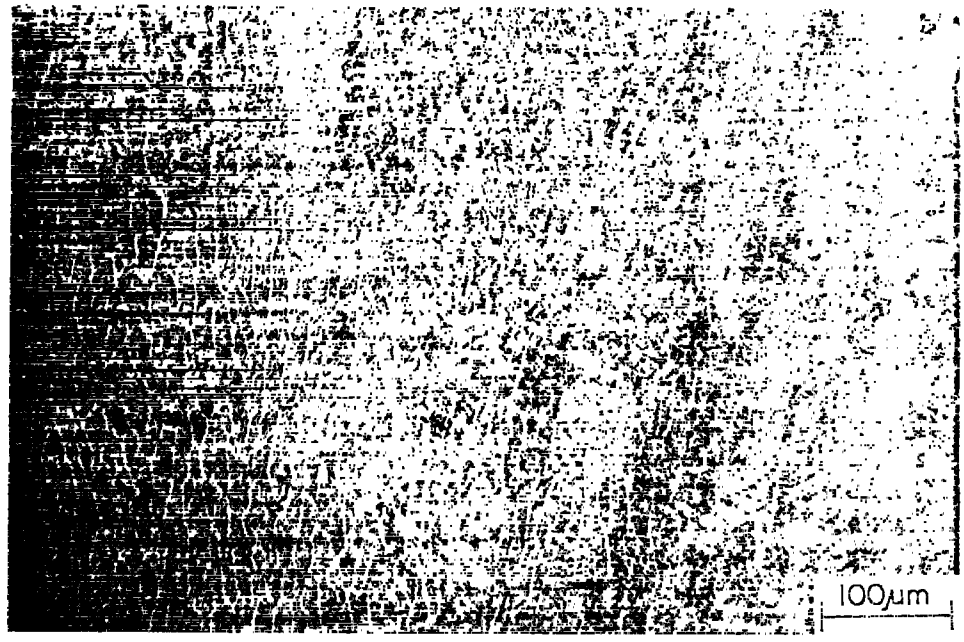

Fig. 22b — Predominantly dendritic structure near the fracture edge in specimen R

HY-130 SMA Weldment (Specimen E)

Macroscopic examination of specimen E, the as-welded, SMA specimen (Fig. 23), disclosed a relatively smooth, flat fracture surface as compared to that of specimen R, a GMA as-welded specimen. In some areas large facets were found adjacent to the columnar grains, whereas in other areas the fracture surface looked smooth and fine textured. Secondary cracks were found in the vicinity of the fatigue/SCC interface and also at the SCC/fast-fracture interface. In the root pass area the surface was rough and irregular, but the sides of the specimen were smooth, showing no indication of embrittlement when examined macroscopically. The fast-fracture area contained internal shear lips, the most prominent of which can be seen in the upper-right quadrant of Fig. 23.

In the SCC zone, fracture occurred by IG separation in some of the faceted and columnar grain areas and by cleavage and MVC elsewhere. The smooth, fine-textured areas fractured by MVC exclusively. Cleavage and stretched zones were found in conjunction with secondary cracks in both the SCC and fast-fracture areas. Although not discernible macroscopically, cleavage along the sides of the specimen indicated some embrittlement in these areas.

In contrast to the microstructure of GMA specimen R, the microstructure of specimen E was a mixture of relatively fine grained, tempered martensite and bainite (Fig. 24). Although chains of precipitates were found in the grain boundaries, there were no discernible cracks within the microstructure, and branching was limited to short, scattered

microcracks along the fracture edge. Also, the solidification substructure along the fracture edge was predominantly fine and cellular and included relatively few solute pools.

The hardness of the weld metal at the fracture edge of specimen E ranged from 33.7 R_c to 36.6 R_c.

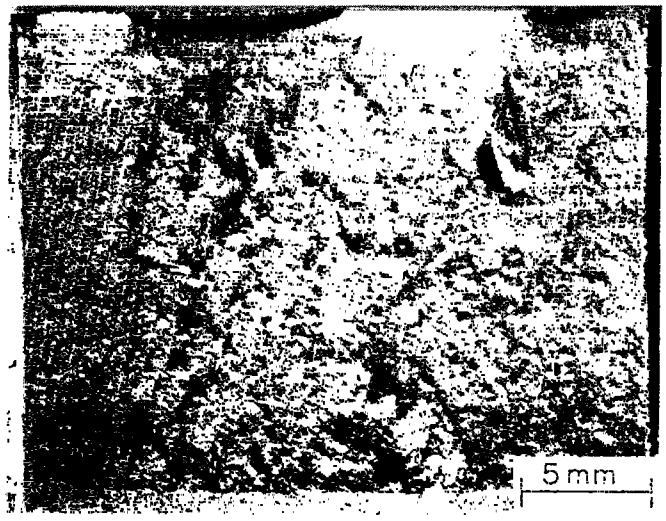

Fig. 23 — Fracture surface of specimen E, the HY-130 SMA weldment

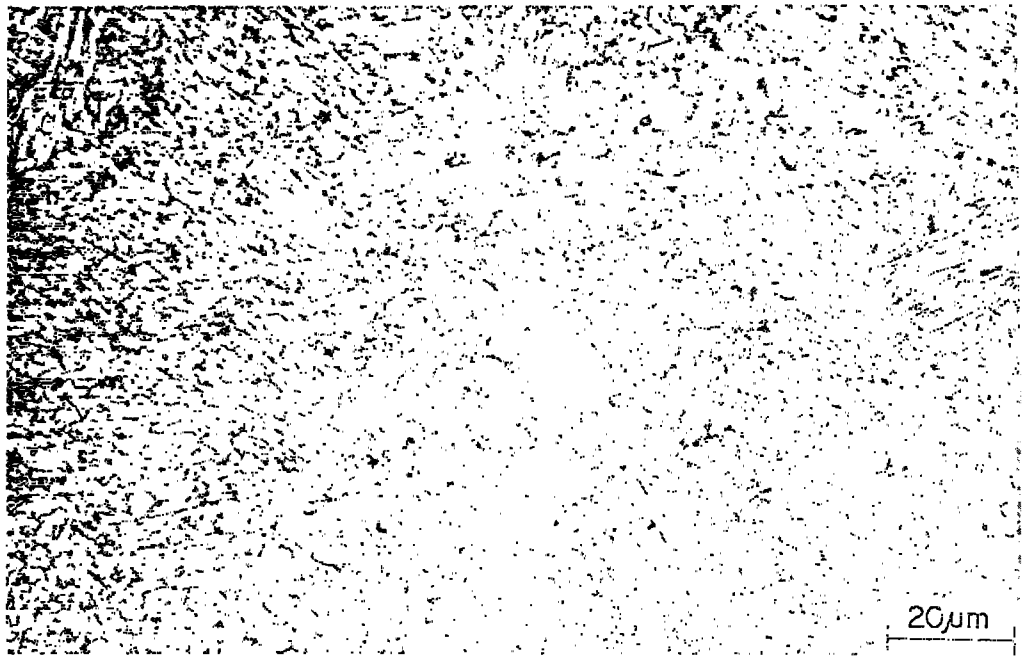

Fig. 24 — Microstructure composed of tempered martensite and bainite in specimen E

HY-180 GTA Weldments (Specimens I, J, Q, and H)

Macroscopic examination showed that the SCC areas in specimens I, J, Q, and H (Figs. 25, 26, 27, and 28) were all generally smooth and fine textured, except for the root pass areas and the surface beads along the sides of the specimens.

Fracture of the smooth SCC area in specimen I, the coarse-bead specimen, occurred predominantly by cleavage. There were, however, small patches of dimples scattered randomly throughout. The cleavage facets in this area were fine and regular in shape. In specimen J, the fine-bead as-welded specimen, fracture of the smooth SCC area occurred by MVC. In both specimens I and J relatively large cleavage facets were found in the SCC areas at the root pass and also along the sides of the specimens. Extensive secondary cracking occurred in the root pass area in specimen I.

Fast fracture in both specimens I and J occurred by MVC. Dimples ranged from fine, equiaxed formations to large, conical formations in specimen I, whereas equiaxed dimples of a relatively uniform size were predominant throughout the fast-fracture area in specimen J.

The tempered specimens, specimens Q and H, showed similar fracture modes in both the SCC and the fast-fracture areas. In the smooth SCC areas fracture occurred by MVC, whereas in the coarse regions, at the centers and sides of these two specimens, fracture occurred by MVC and cleavage. The dimples formed in specimen Q were coarser than those in specimen H, the overtempered specimen.

No evidence of IG separation was found in any of the HY-180 weldments, and no significant amount of secondary cracking was found in the fast-fracture areas.

Metallographic examination of the longitudinal section of specimen I, the smooth SCC area, showed a highly acicular structure of tempered martensite with a second phase, a light etched band of leaflike structure, at the grain boundaries (Figs. 29 and 30). Microprobe analysis showed a slight increase in the concentrations of Ni and Cr within this grain-boundary phase, the hardness of which was 49.5 R_c. The hardness of the acicular structure within the grain was 47.8 R_c.

A uniform microstructure of tempered martensite with a hardness of 46.6 R_c was found along the fracture edge in the longitudinal section of specimen J (Fig. 31). The microstructures of the heat-treated specimens, specimens Q and H, were similar in appearance to that of the grain-boundary phase in specimen I (Figs. 32 and 33). Specimen Q contained light and dark etched areas with hardnesses of 49.3 R_c and 48.1 R_c respectively. The microstructure of the overtempered specimen, specimen H, was finer than that of Q and considerably softer, with a hardness of 39.1 R_c.

In the as-welded specimens, specimens I and J, the center of the weldment or root pass area, which was included in the transverse section, consisted of a coarse columnar structure showing relatively little tempering. The smooth SCC zone showed varying degrees of tempering and grain refinement depending on the extent of thermal cycling. In a progression outward toward the edge of the specimen, the microstructure became increasingly coarse as the number of thermal cycles decreased. The coarsest untempered columnar structure was found in the final uncycled weld beads at the sides of the specimens. In general a similar

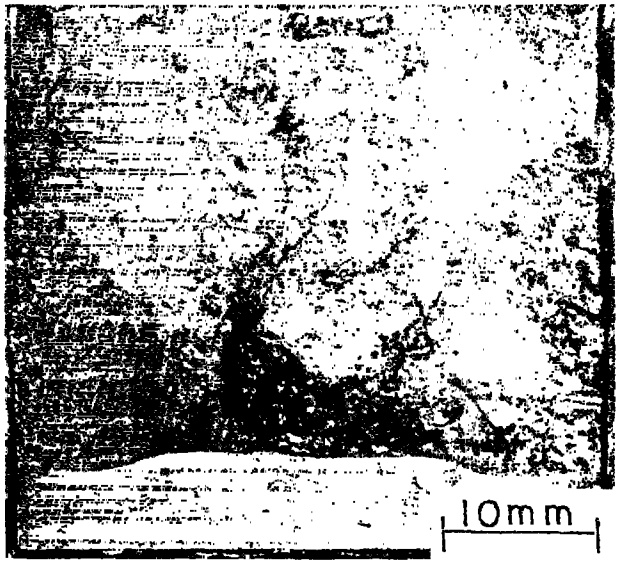

Fig. 25 — Fracture surface of specimen I, the HY-180 coarse-bead, as-welded, GTA weldment

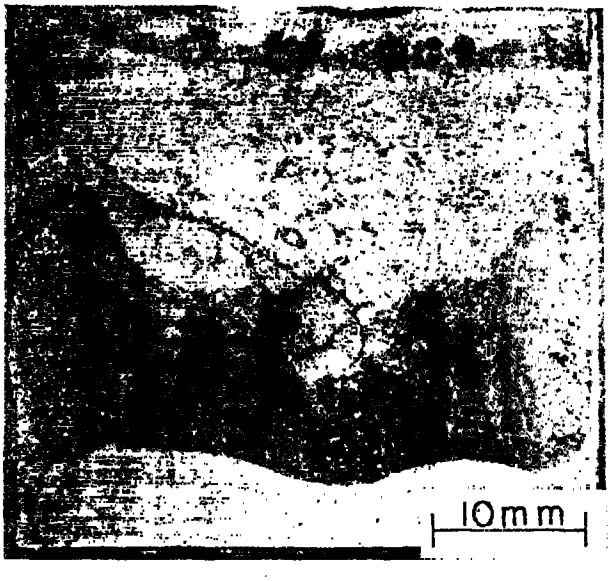

Fig. 26 — Fracture surface of specimen J, the HY-180 fine-bead, as-welded, GTA weldment

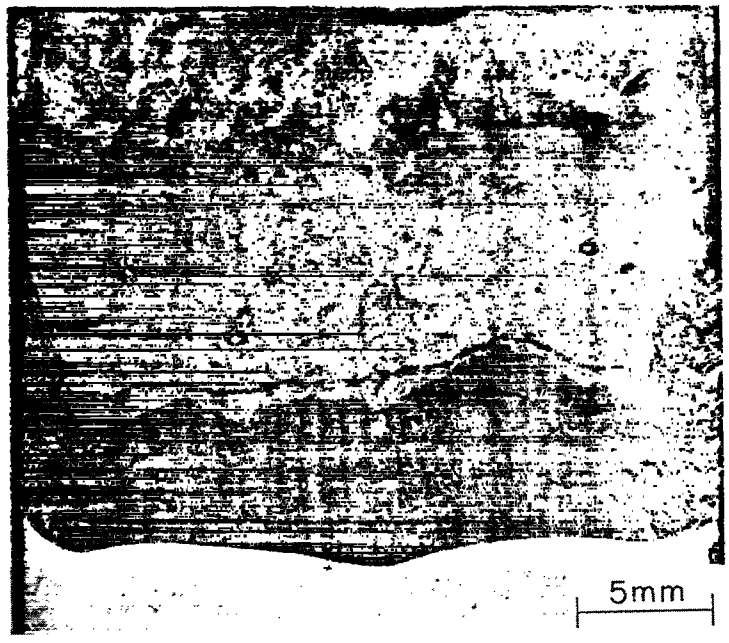

Fig. 27 — Fracture surface of specimen Q, the HY-180 fine-bead tempered weldment

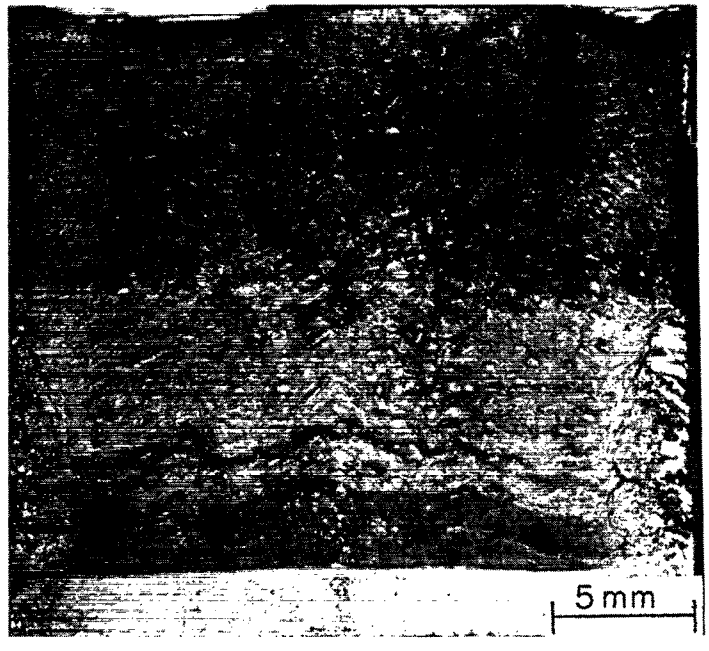

Fig. 28 — Fracture surface of specimen H, the HY-180 fine-bead overtempered weldment

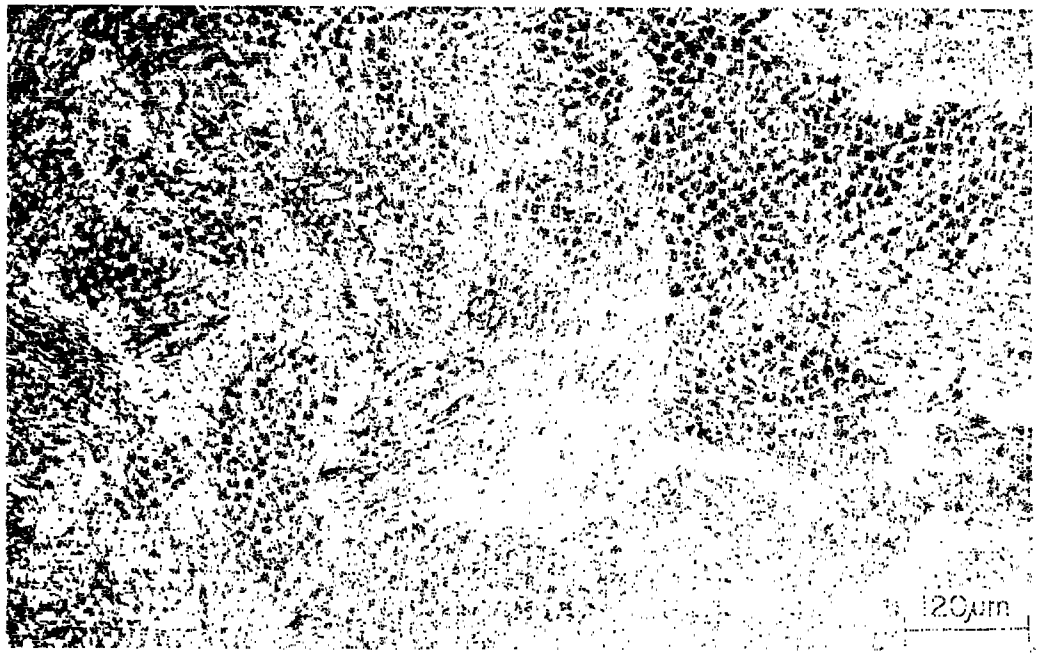

Fig. 29 — Macrostructure showing a light etched grain-boundary phase in specimen I, etched with Kalling's reagent

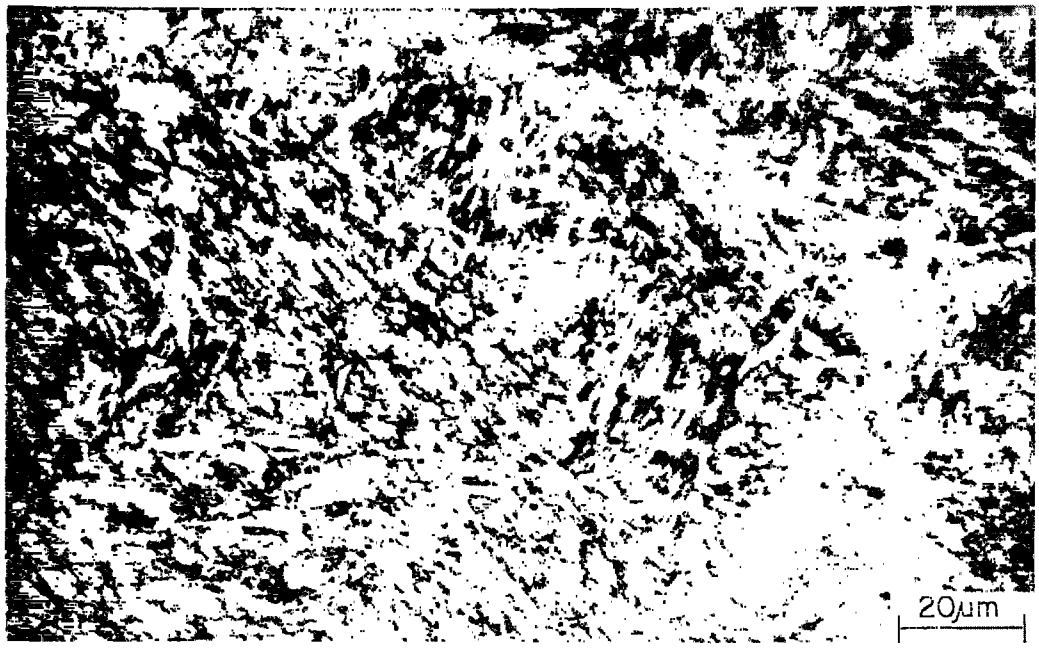

Fig. 30 — Microstructure in specimen I showing an acicular structure within the grains and the leaflike structure of the grain boundary phase seen in Fig. 29

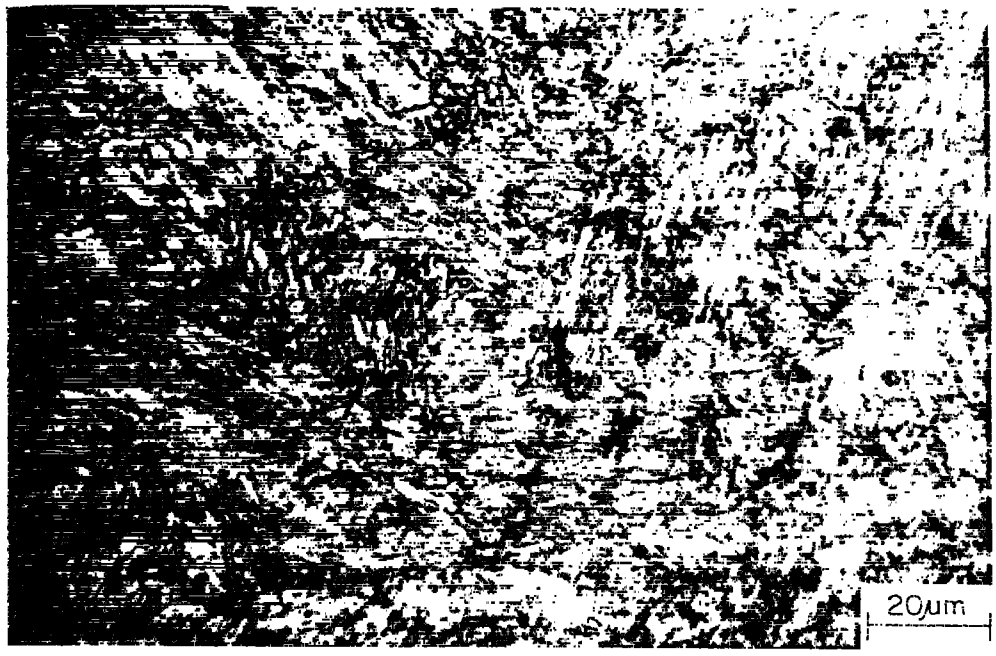

Fig. 31 — Tempered martensitic microstructure in specimen J

Fig. 32 — Fine-grained, tempered structure in specimen Q, a heat-treated HY-180 specimen

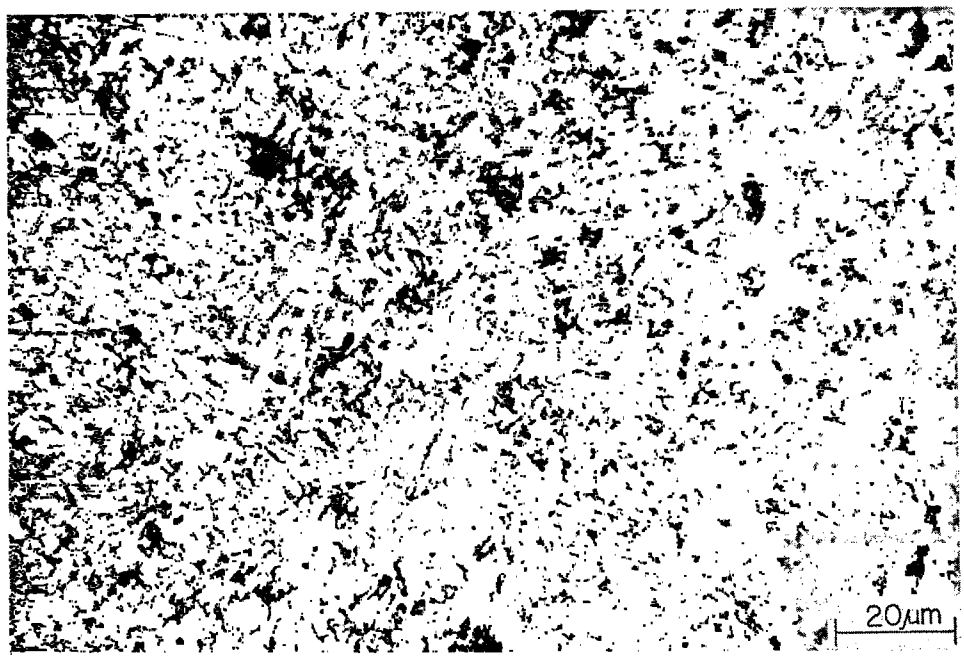

Fig. 33 — Fine-grained microstructure in specimen H, the overtempered HY-180 specimen

progression of microstructures was found in all of the transverse sections of the as-welded specimens analyzed.

The metallographic sections of all four of the HY-180 specimens contained secondary cracks in the SCC zones. In addition to microcracks originating at the fracture edge and extending vertically into the microstructure, specimen I contained short, broad, blunt microcracks. In specimen J the microcracks were finer and appeared in some instances to be associated with chainlike formations of precipitated particles throughout the microstructure. Far fewer microcracks were found in specimens H and Q, the tempered specimens. Those that had occurred were short, sharp cracks originating at the fracture edge.

DISCUSSION

In the as-welded specimens the irregular shape of the SCC zone is related to the microstructure, which is governed in turn by the degree of thermal cycling of the weld metal. Variations in the microstructure throughout the weldment are best illustrated in transverse metallographic sections of the as-welded specimens.

For the most part a coarse-grained, untempered microstructure develops in the final passes during fabrication of the weldment. Subsequent exposure of this area to the corrosive environment during SCC testing results in embrittlement, as evidenced by intergranular fracture and coarse cleavage along the sides of the as-welded specimens. The crack front

advances more rapidly in this area than in most of the remaining weld metal, where the microstructure is generally refined and tempered due to repeated thermal cycling and where exposure of a fresh surface to the corrosive medium is restricted by the crack opening. The exception is in the root pass area. Here, thermal cycling is minimal, and the microstructure shows relatively little tempering. Fracture in this area usually occurs by coarse cleavage and/or IG separation as well as MVC. Also, a slight bulge is often observed macroscopically in the crack front in the root pass area. This bulge indicates more rapid advancement of the propagating crack at this location than in the adjacent thermally cycled areas, where MVC is generally the predominant fracture mode.

Tempering of the as-deposited weld metal reduces its susceptibility to embrittlement. The result is a generally smooth SCC zone of relatively uniform depth which may fracture exclusively by MVC. Tempering generally increases the K_{Iscc} value relative to that of the as-deposited weld metal, as seen in Table 1.

In the as-deposited weld metal the GTA welds exhibit the least amount of low-energy fracture. Repeated thermal cycling, due to the number of passes required to fabricate these find-bead weldments, results in a generally refined, tempered microstructure. On the other hand the coarse beads in the GMA and SMA weldments undergo less thermal cycling during fabrication. The result is the formation of a coarse-grained, relatively nonuniform microstructure. The slower cooling rate of the coarse-bead welds may also result in the formation of high-temperature-transformation products, certain morphologies of which have been reported to be susceptible to embrittlement and cracking [4].

In the HY-130 system the fine-bead (GTA) specimen (specimen T) and the heat-treated, coarse-bead (GMA) specimen (specimen K) showed a similar high resistance to SCC. Both weldments were fabricated with electrodes of base-metal composition rather than with the conventional, higher strength welding electrode. Although the smooth SCC areas of specimen T fractured by MVC, specimen K exhibited a considerable amount of low-energy fracture, which would indicate lower resistance to SCC.

A comparison of the microstructures shows a fine, uniform subgrain structure in the thermally cycled region of specimen T (Fig. 10). Prior austenite grains cannot be discerned. In specimen K a coarser overall grain size is apparent. However, a relatively fine and uniform structure—in this case acicular—still exists within the prior austenite grains (Fig. 17). The microstructure of specimen G, an as-deposited, GMA specimen (Fig. 16), is a coarse-grained mixture of blocky and acicular ferrite. Heat treating refined the grain size and altered the microstructure sufficiently to improve the resistance of the weld metal to SCC.

In the HY-180 system the coarse-bead as-welded specimen (specimen I) fractured by cleavage, whereas the fine-bead as-welded specimen (specimen J) fractured by MVC. Here again the two weldments offered comparable resistance to SCC. Again the microstructure of I (Fig. 30) within the prior austenite grains, although predominantly acicular, is relatively fine and uniform. Overtempering the fine-bead as-welded specimen to a lower yield strength (specimen H) resulted in a uniform, fine-grained, tempered microstructure which offered the greatest resistance to SCC.

The K_{Iscc} values of HY-130 GTA specimen F, HY-130 GMA specimen R, and the HY-130 SMA specimen, specimen E, are also comparable. The microstructure of specimen F is uniform and fine grained, and the specimen fractured by MVC.

HY-130 specimens E and R, on the other hand, are both composed of coarser grained, mixed microstructures and exhibited substantial amounts of low-energy fracture and microbranching of the main crack. In these two specimens the occurrance of patches of bainite and ferrite in the microstructure probably provided the additional paths susceptible to microfracture which resulted in crack branching.

In an investigation of subcritical crack growth in Ti alloys, Williams [5] observed that crack branching occurring on a small scale as relatively short, fine microcracks relieves the stress concentration at the crack tip and that crack arrest may follow. To reinitiate crack growth after arrest, a greater load must be applied than that required to sustain uninterrupted crack growth; consequently K_{Iscc} values will be relatively high.

Comparison of the microstructural features of the two HY-130 as-welded GTA specimens shows that some microbranching occurred in specimen T but was virtually nonexistent in specimen F, although the microstructures viewed optically are similar.

In the HY-100 system, the GTA and the GMA specimens again show similar K_{Iscc} values, although the GMA specimen (specimen A) exhibited more low-energy fracture and a less uniform microstructure. A prominent, ferritic network, however, formed at the prior austenite grain boundaries in the GMA weldment, and microbranching occurred. On the other hand, the more uniform microstructure of the GTA weldment (specimen Z) did not lend itself to microbranching.

An attempt was made to correlate the K_{Iscc} values with the observed macrostructural and microstructural characteristics of the welds. In each alloy (HY-100, HY-130, and HY-180) a numerical rating was assigned to each weld for each of the following categories: the hardness values near the fracture surface (low to high), the fracture separation mode (MVC, cleavage, and IG), the uniformity of the microstructure (most to least uniform), the microstructural transformation products according to transformation temperature (lowest to highest temperature), the amount of branching observed on the fracture surface (least to most), and the degree of smoothness of the macrofracture surface (smooth to coarse). By summing the ratings for each weldment, the following ranking was obtained: In the HY-100 welds, specimen Z was better than specimen A, in the HY-130 welds, the order was T, F, K, E, G, R, L, and in the HY-180 welds the order was H, Q, J, I. In the HY-180 welds this ranking is identical to a ranking based on K_{Iscc} values; in the HY-130 welds the ranking obtained from the K_{Iscc} values is T, K, E, R, G, F, L; and in the HY-100 welds the ranking is A, Z. Thus, whereas some general correlations can be made, the correlation matrix is not isomorphic.

CONCLUSIONS

The following is concluded:

- In general a uniform, fine-grained, tempered microstructure offers the greatest resistance to stress-corrosion cracking;
- The uniformity of the microfracture process, whether it occurs by MVC or by cleavage, may be of greater significance than the fracture mode per se;

- A microstructure providing alternate crack paths that give rise to microbranching of the advancing crack front may result in a relatively high K_{Iscc} value as determined by accelerated laboratory tests.

REFERENCES

1. C.T. Fujii, F.W. Fraser, and E.A. Metzbower, "Stress-Corrosion Cracking Characterization of High-Strength Steels—Base Metals and Weldments," NRL Report 8230, May 1978.

2. B.F. Brown, "A New Stress-Corrosion Cracking Test for High Strength Alloys," Materials Research and Standards 6 (No. 3), 129-133 (1966).

3. F.W. Fraser, E.A. Metzbower, and J. Stoop, "A Correlation Between SCC Path, Hardness, Microstructure, and Microsegregation in HY-130 E14018 Weld Metal," NRL Report 8193, Dec. 1978.

4. T. Boniszewski and F. Watkinson, "Effect of Weld Microstructures on Hydrogen-Induced Cracking in Transformable Steels: Part II," Metals and Materials 7, 145-151 (Mar. 1973).

5. D.N. Williams, "Subcritical Crack Growth Under Sustained Load," Met. Trans. 5, 2351-2358 (Nov. 1974).